NASA TECHNICAL NOTE

NASA TN D-4681

NASA TN D-4681

STRIKING CHARACTERISTICS OF THE MAGNETRON IONIZATION GAGE IN HELIUM FROM 1.9×10^{-7} TORR TO 7×10^{-10} TORR

by William S. Lassiter

Langley Research Center
Langley Station, Hampton, Va.

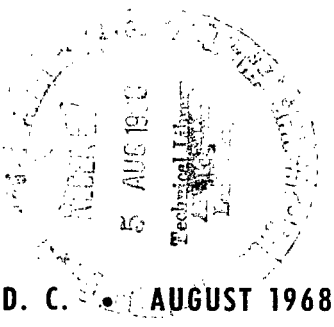

NATIONAL AERONAUTICS AND SPACE ADMINISTRATION • WASHINGTON, D. C. • AUGUST 1968

NASA TN D-4681

STRIKING CHARACTERISTICS OF THE MAGNETRON IONIZATION GAGE IN HELIUM FROM 1.9×10^{-7} TORR TO 7×10^{-10} TORR

By William S. Lassiter

Langley Research Center
Langley Station, Hampton, Va.

NATIONAL AERONAUTICS AND SPACE ADMINISTRATION

For sale by the Clearinghouse for Federal Scientific and Technical Information
Springfield, Virginia 22151 – CFSTI price $3.00

STRIKING CHARACTERISTICS OF THE MAGNETRON IONIZATION GAGE IN HELIUM FROM 1.9×10^{-7} TORR TO 7×10^{-10} TORR

By William S. Lassiter
Langley Research Center

SUMMARY

The striking characteristics of the magnetron gage were measured in helium over a pressure range of 1.9×10^{-7} torr (N_2) $(25.3\ \mu N/m^2)$ to 7×10^{-10} torr (N_2) $(93.1\ nN/m^2)$. The measured striking characteristics on the upper branches of the striking characteristics diagram agree with the Townsend discharge theory except that, for a given pressure, the characteristics deviate slightly from the theoretical parabolic prediction. On the lower branches, a significant disagreement with theory was found to exist in the dependence of the minimum striking voltage with pressure. Otherwise, on the lower branches, the measured striking behavior agrees with the theoretical prediction and with measurements at higher pressures. Measured striking-time lags occurred in the magnetron gage at pressures below 5×10^{-8} torr (N_2) $(6.65\ \mu N/m^2)$. The lags were determined to cause no significant error in the measurements of the striking characteristics.

INTRODUCTION

The extension of space simulation capabilities to lower pressures requires a simultaneous extension of the capability to measure pressures in the ultrahigh vacuum (UHV) region. One of the devices currently being used in this pressure region in space-simulation chambers is the magnetron gage.

Measurements of the lower limits of the anode voltage and magnetic field at which the gage will operate (striking characteristics) should give data which aid in the understanding of the nature of the discharge within the gage. A knowledge of the discharge phenomena will permit one to minimize the well-known (ref. 1) nonlinearity of the ion current-pressure relationship in the ultrahigh vacuum region.

The magnetron gage was developed by Redhead (ref. 1) in 1958. Redhead (ref. 1) and other authors (refs. 2 and 3) have reported calibration studies of the magnetron gage in the ultrahigh vacuum region, but no data are available on the striking characteristics in helium below 1.9×10^{-7} torr (N_2) $(25.3\ \mu N/m^2)$. The purpose of this paper is to present data of measurements of the striking characteristics of the magnetron gage in helium

from 1.9×10^{-7} torr to 7×10^{-10} torr (N_2). Helium, a gas commonly used as a test gas in the calibration of vacuum gages, was chosen because of its inertness. Secondary electron-emission coefficients and striking-time lags are also presented.

SYMBOLS

Some of the physical quantities defined herein are given both in the International System of Units (SI) and the U.S. Customary System. The factors relating these two systems of units are presented in reference 4.

a,b,c,d,k	constants
B	magnetic flux density, gauss
D	diameter of rolling circle generating a cycloid, centimeters
e	electronic charge, electrostatic units
E	electric field strength, volts per centimeter
i	current reaching the anode, amperes
i_o	current released from cathode by ultraviolet illumination, amperes
l	distance between cathode end plates, centimeters
m	mass of electron, grams
n	number of ions and/or electrons
p	pressure, torr
r	radius from longitudinal axis of cylindrical portion of cathode to some point between anode and cathode, centimeters
r_1	maximum radius at which ionization can occur, centimeters
t	time, minutes
t_m	measured striking-time lag, minutes

v	electron total velocity, centimeters per second
v_r	electron rotating velocity, centimeters per second
v_θ	electron drift velocity, centimeters per second
V	voltage, volts
V_i	ionization potential, volts
W_{max}	maximum kinetic energy of an electron, electron-volts
α	first Townsend coefficient, ion pairs per centimeter per electron
γ	secondary electron emission coefficient, electrons per ions
Γ	effective second Townsend coefficient, electrons per ion
λ	electron mean free path, centimeters
ψ	probability of an electron-gas molecule collision
$\psi' = 1 - \psi$	
η	electronic charge to mass ratio, e/m, electrostatic units per gram

Subscripts:

a	conditions at inner surface of anode
e	conditions at inner surface of cathode end plates
k	conditions at outer surface of cylindrical portion of cathode
s	striking conditions
min	minimum

Arrows over symbols indicate vectors.

MAGNETRON DESCRIPTION AND THEORY

Geometry of Magnetron Gage

The physical arrangement of the magnetron gage is shown in figure 1. Table I (from ref. 1) presents the salient dimensions. The spool-like cathode consists of a hollow cylinder with a disk attached to each end. These disks are referred to as the cathode end plates. The anode is a perforated hollow cylinder surrounding the cathode. Two annular electrodes, the auxiliary cathodes, are inserted between the anode and the cathode end plates and are maintained at ground potential to shield the cathode end plates from high electric fields. A radial electric field E is produced by the voltage gradient between the anode (at potential V_a) and the cathode (at ground potential). A uniform magnetic field B is applied in the axial direction.

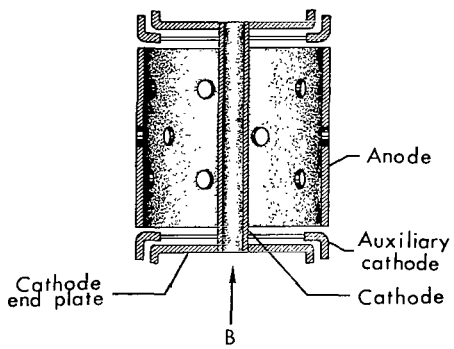

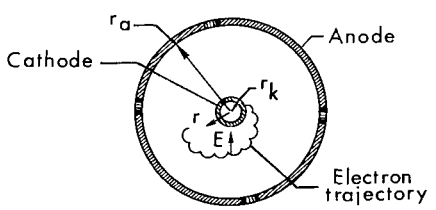

Figure 1.- Magnetron electrode arrangement.

TABLE I.- DIMENSIONS OF MAGNETRON TEST GAGE

Anode radius, r_a, mm	15
Anode length, mm	14
Cathode radius, r_k, mm	1.45
Cathode length, l, mm	20

Striking Characteristics

The striking characteristics of the magnetron gage are the minimum values of (1) the anode voltage for a given magnetic field and (2) the magnetic field for a given anode voltage required to initiate a self-sustaining discharge within the gage at a given pressure. The initiation of this self-sustaining discharge will hereafter be referred to as breakdown. Once the striking characteristics have been applied, the gage is in operation.

Regions of Operation

The voltage and magnetic field requirements for the operation of the magnetron gage can be best described by referring to a plot of the theoretical striking characteristics. (See fig. 2.) At high anode voltages and low magnetic fields, the discharge is maintained primarily by secondary electron emission from the cylindrical portion of the cathode. This type of discharge is very similar to the well-known Penning discharge and the region in which this discharge exists will hereafter be referred to as region a. This region contains the upper branches of the striking characteristics curves. (See fig. 2.)

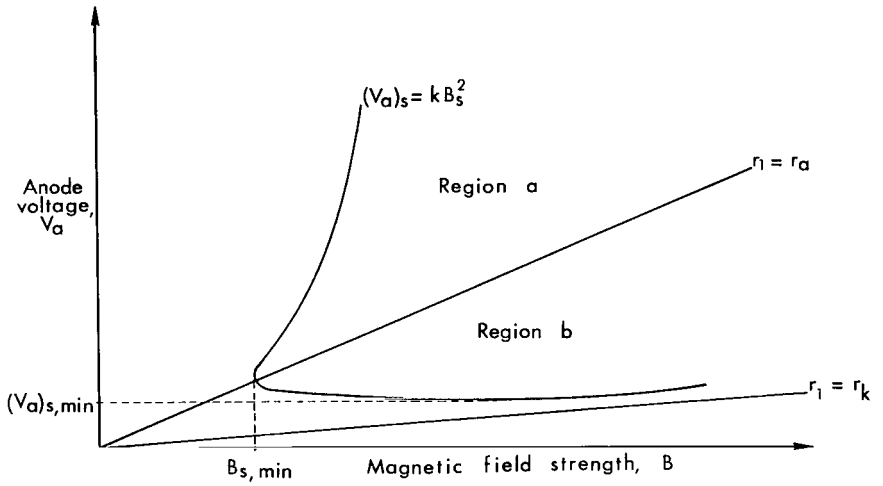

Figure 2.- Theoretical striking characteristics diagram.

At high magnetic fields and low anode voltages where the Penning discharge cannot occur, the discharge of the magnetron gage is sustained by secondary electron emission from the cathode end plates. (See ref. 1.) The region in which this type of discharge occurs will hereafter be referred to as region b and contains the lower branches of the striking characteristics curves. (See fig. 2.)

Theory of Townsend Breakdown Criterion

The theory of breakdown for the magnetron gage is based on the theory presented by Redhead (ref. 5) for a Townsend discharge in a coaxial diode with axial magnetic field. The theory describing the conditions for breakdown is reviewed in this section. Supplementary information describing electron trajectories and first and second Townsend coefficients is reviewed in appendix A.

The theory of breakdown for the magnetron gage is based on the assumptions of no space charge buildup between the electrodes and no effects on the electric field from the

cathode end plates. The assumption of a constant electric field over each cycloid of an electron trajectory is also made. Because of this assumption, the theory is often referred to as the constant-field theory. The electric field throughout the interelectrode spacing of the magnetron gage is nonuniform and is

$$E = \frac{V_a}{r \log_e \frac{r_a}{r_k}} \tag{1}$$

Multiplying each side of equation (1) by r and evaluating the resulting expression at r_k yields

$$r_k E_k = rE \tag{2}$$

The Townsend breakdown criterion for nonuniform electric fields is (see appendix A)

$$\int_{r_k}^{r_1} \alpha \, dr = \log_e\left(1 + \frac{1}{\Gamma}\right) \tag{3}$$

The expression derived by Redhead (ref. 5) for the first Townsend coefficient

$$\alpha = \frac{3E}{\frac{4E^2}{\eta B^2} + eV_i} \tag{4}$$

is substituted into equation (3). Integration of equation (3) and use of equation (2) yields

$$\log_e\left(1 + \frac{1}{\Gamma}\right) = \frac{3r_k E_k}{2eV_i} \log_e\left[1 + \frac{\eta V_i}{4}\left(\frac{rB}{r_k E_k}\right)^2\right]_{r_k}^{r_1} \tag{5}$$

The upper limit of the evaluation of equation (5) r_1 may assume two values, one being the anode radius and the other being some radius less than the anode radius (ref. 5).

Region a.- When the upper limit of equation (5) is equal to the anode radius, secondary electron emission from the cylindrical portion of the cathode controls the discharge and, once the striking characteristics are applied, the gage operates in region a. In this region, ionization can occur anywhere within the interelectrode spacing between r_k and r_a. With the use of $r_1 = r_a$ as the upper limit in equation (5) and by assuming

$\left(B/E_k\right)^2 \ll 1$, expanding $\log_e\left[1 + \frac{\eta V_i}{4}\left(\frac{rB}{r_k E_k}\right)^2\right]$ in equation (5), and retaining first-order terms, the striking voltage in region a can be found from equation (5) to be

$$\left(V_a\right)_s = \frac{\frac{3}{8} B_s{}^2\left(r_a{}^2 - r_k{}^2\right)\log_e \frac{r_a}{r_k}}{\log_e\left(1 + \frac{1}{\Gamma_k}\right)} \tag{6}$$

Equation (6) is shown schematically in region a of figure 2 and predicts a parabolic dependence of the striking voltage on the striking magnetic field. If Γ_k in equation (6) is assumed to be constant, the ratio $\left(V_a\right)_s/B_s{}^2$ is constant.

In order to cause ionization leading to breakdown, electrons emitted from the cylindrical portion of the cathode or formed in the interelectrode spacing must have a maximum kinetic energy W_{max} while traversing a cycloid, at least equal to the ionization potential of the gas present, or

$$W_{max} \geqq eV_i \tag{7}$$

The maximum kinetic energy W_{max} can be shown to be (ref. 1)

$$W_{max} = ED \tag{8}$$

The minimum requirements for ionization are that

$$W_{max} = ED = eV_i \tag{9}$$

With the use of equation (1) and the expression for D (ref. 1)

$$D = \frac{2E}{\eta B^2} \tag{10}$$

equation (9) can be solved to yield

$$\left(V_a\right)_{r_1=r_a} = \left(\frac{e\eta V_i}{2}\right)^{1/2} r_a B \log_e \frac{r_a}{r_k} \tag{11}$$

Equation (11) describes the lower limit of region a and is shown schematically in figure 2 as the line at which $r_1 = r_a$. The point at which the line described by equation (11) intersects the striking characteristics curve in region a (eq. (6)) is the point at which the

minimum striking magnetic field occurs in region a. This minimum striking magnetic field can be found by setting equation (6) equal to equation (11) and solving for B. This procedure yields

$$B_{s,min} = a \log_e \frac{b}{p} \tag{12}$$

(see fig. 2) where pressure is used instead of Γ_k. (See appendix A for the dependence of Γ_k on pressure.)

Region b.- In region b, the probability of ionization by electrons emitted from the cylindrical portion of the cathode is essentially zero, and the discharge is controlled by the secondary electron emission from the cathode end plates. The upper limit of equation (5) now becomes equal to some maximum radius, less than r_a, at which ionization can occur. This radius can be found by use of the minimum requirements of ionization (expressed by eq. (8)), along with the expression

$$(rE)_{r=r_1} = r_k E_k \tag{13}$$

to be

$$r_1 = \left(\frac{2}{eV_i\eta}\right)^{1/2} \frac{r_k E_k}{B} \tag{14}$$

Use of this limit in the breakdown equation (eq. (5)) yields for the striking voltage in region b

$$(V_a)_s = \frac{\frac{2}{3} V_i \log_e \frac{r_a}{r_k} \log_e\left(1 + \frac{1}{\Gamma_e}\right)}{\log_e \frac{3/2}{1 + \frac{\eta V_i}{4}\left(\frac{B_s}{E_k}\right)^2}} \tag{15}$$

Equation (15), at constant Γ_e, is shown schematically in region b of figure 2.

By the same analysis that was used to express the lower limit of region a, the lower limit of region b can be shown to be

$$(V_a)_{r_1=r_k} = \left(\frac{e\eta V_i}{2}\right)^{1/2} r_k B \log_e \frac{r_a}{r_k} \tag{16}$$

This line is shown schematically in region b of figure 2 (as indicated by $r_1 = r_k$) and represents the line at and below which no ionization causing breakdown within the magnetron gage is possible.

In region b of figure 2, the theoretical striking voltage decreases to a minimum and then increases as B_s increases. The expression for the minimum striking voltage is (refs. 5 and 6)

$$\left(V_a\right)_{s,min} = c \log_e \frac{d}{p} \tag{17}$$

(see fig. 2) where p is used instead of Γ_e. (See appendix A for the dependence of Γ_e on p.)

Application of Theory

The Townsend breakdown criterion has been used to show the theoretical prediction of the minimum values of anode voltage and magnetic field (striking characteristics) required to initiate a self-sustaining discharge at low pressures in a coaxial electrode geometry with cathode end plates. (See eqs. (6) and (15).) The experimental procedure is to measure the striking characteristics of the magnetron gage in high and ultrahigh vacuum region where no data are available and to compare these results with theoretical predictions and results at higher pressures.

Also involved in the experiment are the measurements of the minimum striking magnetic field in region a (theoretically predicted by eq. (12)) and the minimum striking anode voltage in region b (theoretically predicted by eq. (17)). These measurements are compared with the theoretical predictions. The lower limits of regions a and b are calculated from equations (11) and (16), respectively, for the case of helium as the test gas and are plotted with the measured striking characteristics.

DESCRIPTION OF APPARATUS

A schematic of the vacuum system used for this experiment is shown in figure 3. Four magnetron vacuum gages were attached to a Z-shaped stainless-steel manifold which was attached by a $1\frac{1}{2}$-inch bakable valve to a 50-liter/second ion pump. The ion pump was backed up by a 5-cubic-foot-per-minute two-stage mechanical roughing pump. As shown in figure 3, a pyrex finger was also attached to the manifold. The finger could be immersed in either liquid nitrogen or liquid helium contained in the dewar flask shown in figure 3 to help pump the system to the lowest pressures. The leak valve mounted to the manifold was used to admit the test gas into the system in order to change the pressure. A complete description of the system can be found in reference 7.

Figure 4 is a photograph of a portion of the system that includes and is above the $1\frac{1}{2}$-inch bakable valve. Hereafter, this portion of the system is referred to as the ultrahigh vacuum system. Also shown in figure 4 are the three stainless-steel permanent

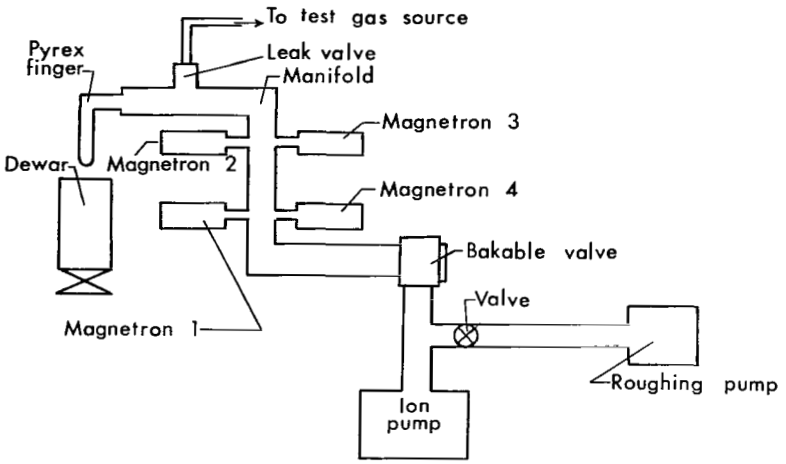

Figure 3.- Schematic diagram of vacuum system used in measurement of striking characteristics.

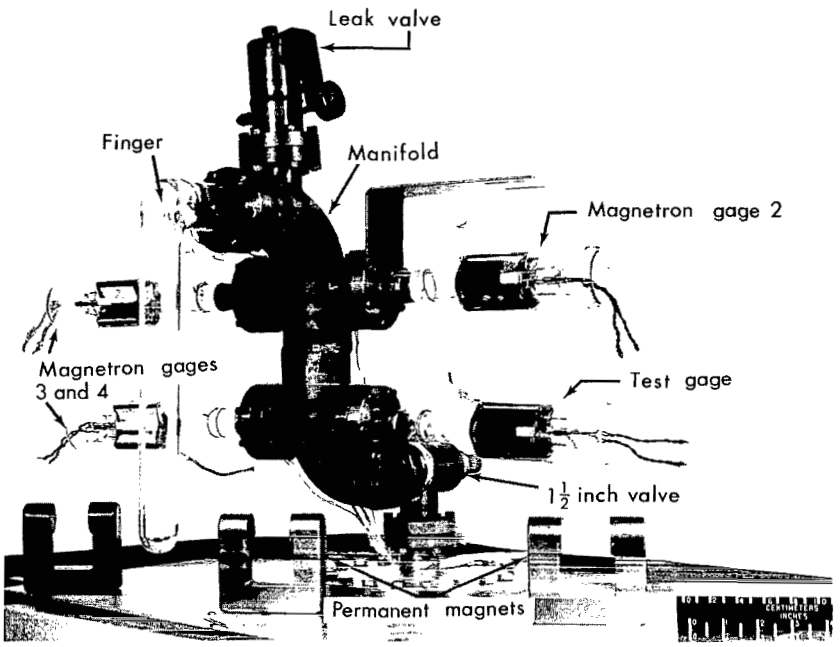

Figure 4.- Ultra-high-vacuum system showing location of magnetron test gage. L-66-7567.1

magnets which are used to provide each of the magnetrons (magnetrons 2, 3, and 4) with a magnetic field of 1050 gauss. The ultrahigh vacuum system shown in figure 4 could be baked up to 450° C.

The entire vacuum system along with gage controllers and other associated equipment is shown in the photograph in figure 5. The gas inlet line extended from the leak

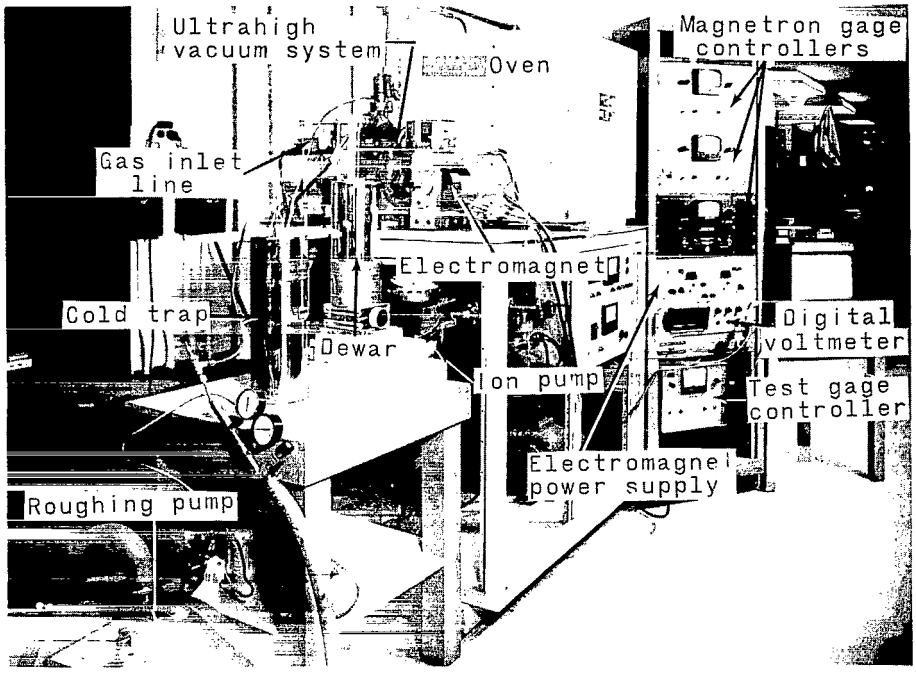

Figure 5.- Vacuum system and associated apparatus. L-66-7569.1

valve on the ultrahigh vacuum system to a stainless-steel tube with outlets to the pressure regulator on the test gas bottle and to a 5-cubic-foot-per-minute roughing pump. Between the roughing pump and stainless-steel tube was a valve which, when closed, isolated the roughing pump from the tube. A portion of the gas inlet line was immersed in a liquid nitrogen cold trap in order to freeze out impurities and to assure that only high purity gas enters the ultrahigh vacuum system. An industrial oven was used to bake the ultrahigh vacuum system. Three magnetron gage controllers were used to supply magnetrons 2, 3, and 4 each with a constant anode voltage of 4800 ± 2.5 volts. These three controllers also measured pressure.

The electromagnet shown in figure 5 supplied a magnetic field to the test gage. The anode voltage for the test gage was supplied by a magnetron gage controller. The controller also indicated the ion current from the test gage. The controller, electromagnet, and digital volt meter were wired so that the test-gage anode voltage and magnetic field were measured by the digital voltmeter. Figure 6 is a diagram showing this method of measurement. The anode voltage to the test gage could be varied from 0 to 7000 volts by the variable autotransformer and test-gage controller. A resistor in the controller was replaced by two variable resistors to enable coarse and fine adjustment of the test-gage anode voltage which was maintained within -1 percent of the initial setting during each

test run. Positioning of the switch enabled the digital voltmeter to measure the anode voltage.

The magnetic field produced by the electromagnet could not be measured during a test run with a gaussmeter, since the test gage was between the pole faces of the electromagnet. Thus, a relatively simple method of measuring the magnetic field during a test run was devised. A 1-ohm resistor (see fig. 6) was placed in series with the electromagnet. Since the magnetic field produced by the electromagnet was directly proportional to the current in the field coils, the magnetic field was also directly proportional to the voltage drop across the resistor. Thus, the magnet was calibrated prior to any test runs by measuring the voltage drop across the 1-ohm resistor and plotting the voltage drop against the magnetic field measured between the pole faces. The magnetic field was measured by a Hall effect gaussmeter with accuracy of ±1 percent of full-scale indication. Proper positioning of the switch shown in figure 6 enabled the voltage drop across the 1-ohm resistor to be measured by the digital voltmeter, which could perform measurements with an accuracy of ±0.1 percent.

All four gages (see fig. 3) were commercial magnetron gages designed according to reference 1. Magnetron gage 1 was used as the test gage. Magnetron gage 2, the response characteristics of which had previously been compared with a calibrated

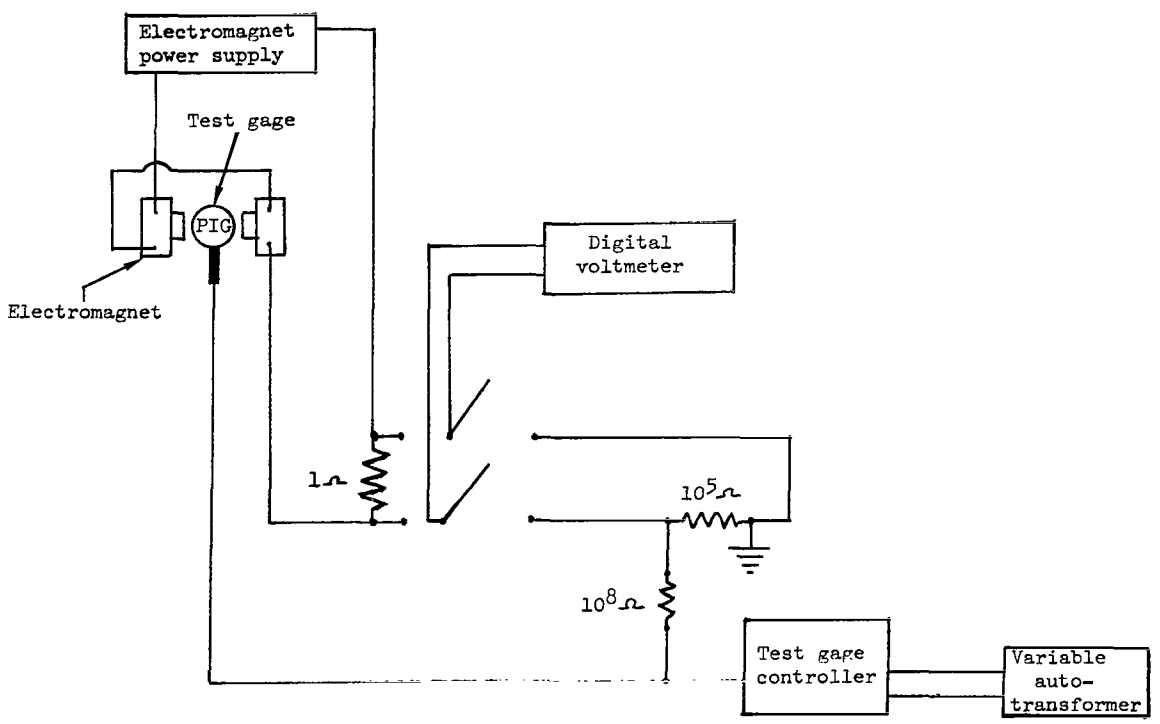

Figure 6.- Diagram of power source, magnetic field supply, readout equipment, and auxiliary wiring for test gage.

modulated hot filament type of ionization gage, was used to measure the total pressure in the system. Accuracy of the comparison and calibration was ±25 percent. Magnetron gages 2, 3, and 4 were used to help pump the ultrahigh vacuum system to lower pressures, after the $1\frac{1}{2}$-inch bakable valve had been closed. The sole purpose of magnetron gages 3 and 4 was to serve as pumps. The magnetron gage has a pumping speed of about 1 liter per second for air (ref. 1) and can be effectively used as a pump in systems with small gas loads.

All tests were performed with research-grade helium as the test gas, with a purity of 99.9995 percent.

PROCEDURE

In order that the outgassing products of the stainless-steel manifold contribute no significant error in the experiment, it was necessary that the system be capable of reaching an ultimate pressure well into the ultrahigh vacuum region at least a decade lower than the lowest test pressure. The following sections describe the procedures for preparing the system for obtaining low pressures and the experimental test procedures.

Cleaning of the System

Since the cleanliness of the system was essential for obtaining low pressures, the ultrahigh vacuum system was given a stringent bake. (See ref. 7.) After the bake the pyrex finger was immersed in liquid nitrogen and the ultimate pressure of the ultrahigh vacuum system was about 3×10^{-11} torr $\left(4 \text{ nN/m}^2\right)$.

Test Procedure

The tests were conducted to determine the striking characteristics of the magnetron gage in helium at pressures from 1.9×10^{-7} torr $\left(N_2\right)$ to 7×10^{-10} torr $\left(N_2\right)$. This section describes the manner in which the tests were conducted.

The test gas was admitted into the system until the pressure was 1.9×10^{-7} torr $\left(N_2\right)$, as measured from magnetron 2. This pressure was held constant throughout the first test. The objective of the first test was to establish the striking characteristics in regions a and b at a pressure of 1.9×10^{-7} torr $\left(N_2\right)$. The lower branch, in region b, of the striking characteristics was measured first by setting a constant magnetic field with the electromagnet, and then varying the anode voltage from zero up to the value at which a self-sustaining discharge occurred in the test gage. The criterion for the establishment of a self-sustaining discharge was the observation of a change in pressure indication on the test-gage controller from approximately 10^{-13} torr (background leakage) to a steady indication of no less than 10^{-11} torr. To establish the upper branch of the striking

characteristics (in region a), a constant voltage was applied and the magnetic field varied from zero up to the value which initiated the self-sustaining discharge. After each point was established in regions a and b, the magnetic and electric fields were decreased to zero so that the discharge would terminate. Data were taken at 1.9×10^{-7} torr (N_2), and 5×10^{-8} torr (N_2) by using the procedure described for establishing the striking characteristics in regions a and b at each test pressure.

The third test was begun after decreasing the pressure in the ultrahigh vacuum system to 1.2×10^{-8} torr (N_2). When investigating region b at this pressure, noticeable time lags of the order of 1 minute occurred between the instant a voltage capable of causing breakdown was applied and the establishment of the discharge within the gage. These time lags occurred at voltages corresponding to and in excess of the true striking voltage. Time lags also occurred at magnetic fields corresponding to and in excess of the true striking magnetic field, but were about a factor of two less than those in region b. Redhead (ref. 1) has reported the observation of striking-time lags of the magnetron gage below 10^{-8} torr, and that as the pressure is decreased, the striking-time lags increase. Thus, to make the time lags shorter, so that the elapsed time would not be enough to cause a change in experimental conditions from pumping by the gages, heating of the electromagnet, and heating of the 1-ohm resistor, the gage was illuminated by a 1-kilowatt mercury lamp during tests at and below 1.2×10^{-8} torr (N_2). The lags were measured by a stopwatch and the primary source of error in the measurement was reflex time. The striking characteristics at these lower pressures were selected to be the anode voltage and magnetic field at which the time lag was greatest. Verification that the mercury lamp did not introduce error in the measurement of the striking characteristics was established by repeating tests with and without use of the mercury lamp. The various values of the striking characteristics found were within the experimental error. More detailed explanation is presented in the section "Results and Discussion" to show that the values of anode voltage and magnetic field selected as the striking values are within a few percent of the true striking characteristics.

RESULTS AND DISCUSSION

In this section the results of the measurements of the striking characteristics of the magnetron gage in helium over the pressure range of 1.9×10^{-7} torr (N_2) to 7×10^{-10} torr (N_2) are graphically presented and discussed. Secondary electron emission coefficients of the cylindrical portion of the cathode are calculated from the striking characteristics and are presented in tabular form. Concluding this section is a discussion and graphical presentation of the striking time lags of the gage.

Figures 7(a) to 7(f) present the results of the measurements of the striking characteristics of the magnetron gage in helium at various pressures over the pressure range

1.9×10^{-7} torr N_2 to 7×10^{-10} torr N_2. Also plotted in these figures for the particular case of helium as the test gas are the lower limits of regions a and b (the lines labeled $r_1 = r_a$ and $r_1 = r_k$), as calculated from equations (11) and (16), respectively. In figure 7 the minimum striking magnetic field in region a for each test pressure is numerically shown as $B_{s,min}$. To show clearly the dependence of the striking characteristics on pressure, the curves at four of the six test pressures are superimposed in figure 7(g). Also shown in figure 7(g) are the manufacturer's recommended operating conditions, an anode voltage and magnetic field of approximately 4800 volts and 1050 gauss, respectively. It is obvious that the recommended operating conditions are well within the lower limits of operation of the gage over the pressure range of the investigation.

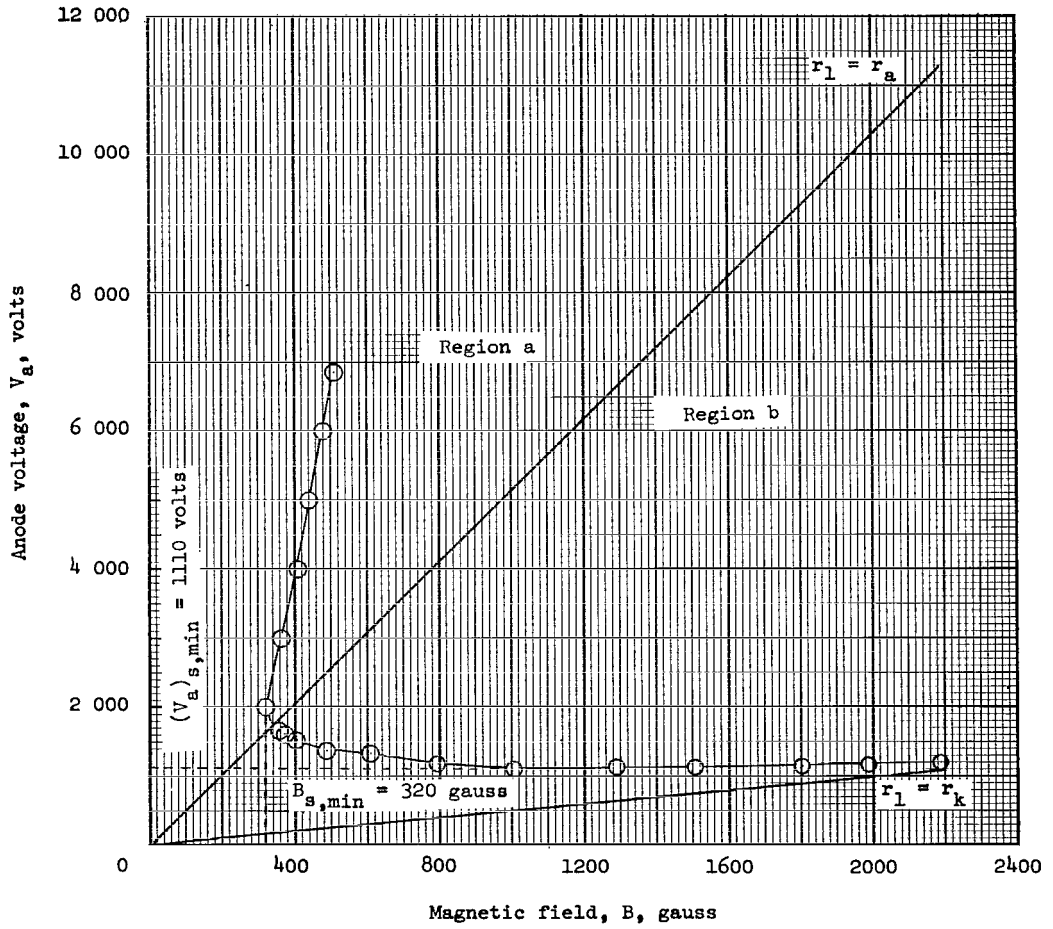

(a) $p = 1.9 \times 10^{-7}$ torr.

Figure 7.- Measured striking characteristics of the magnetron gage in helium.

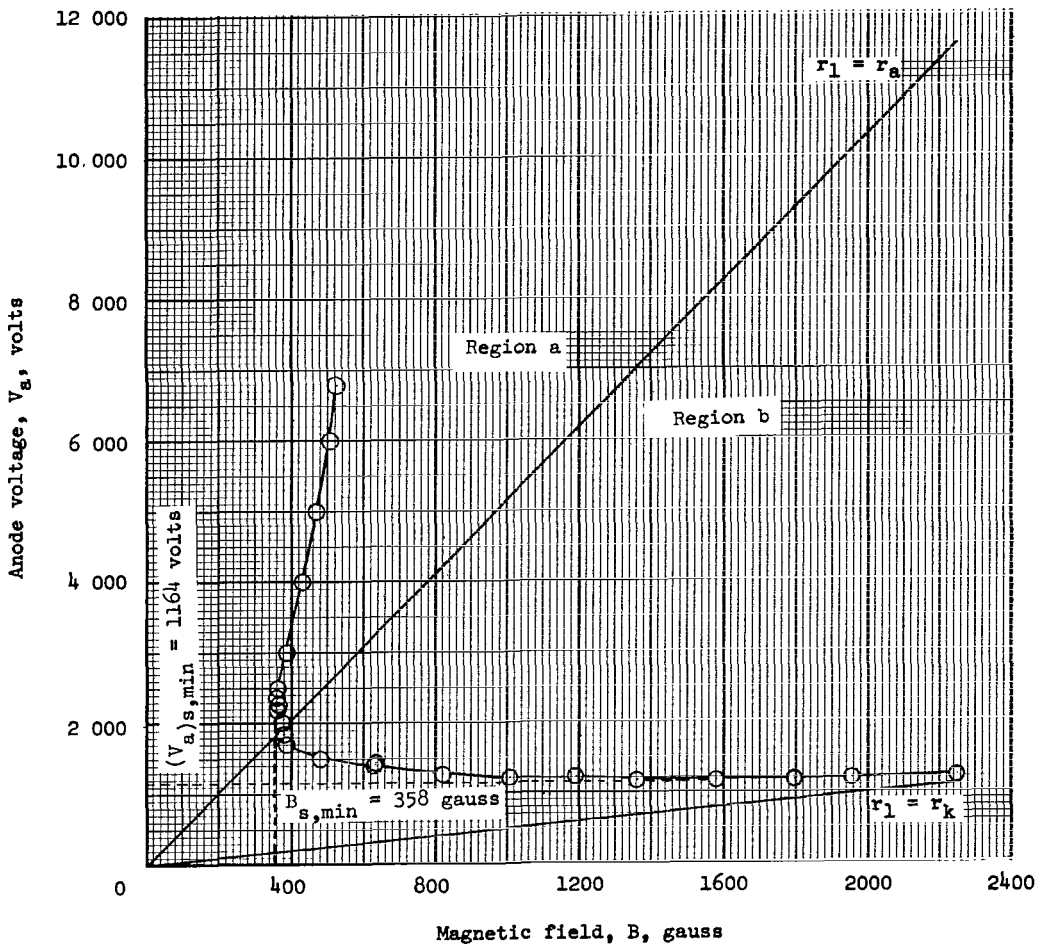

(b) $p = 5.0 \times 10^{-8}$ torr.

Figure 7.- Continued.

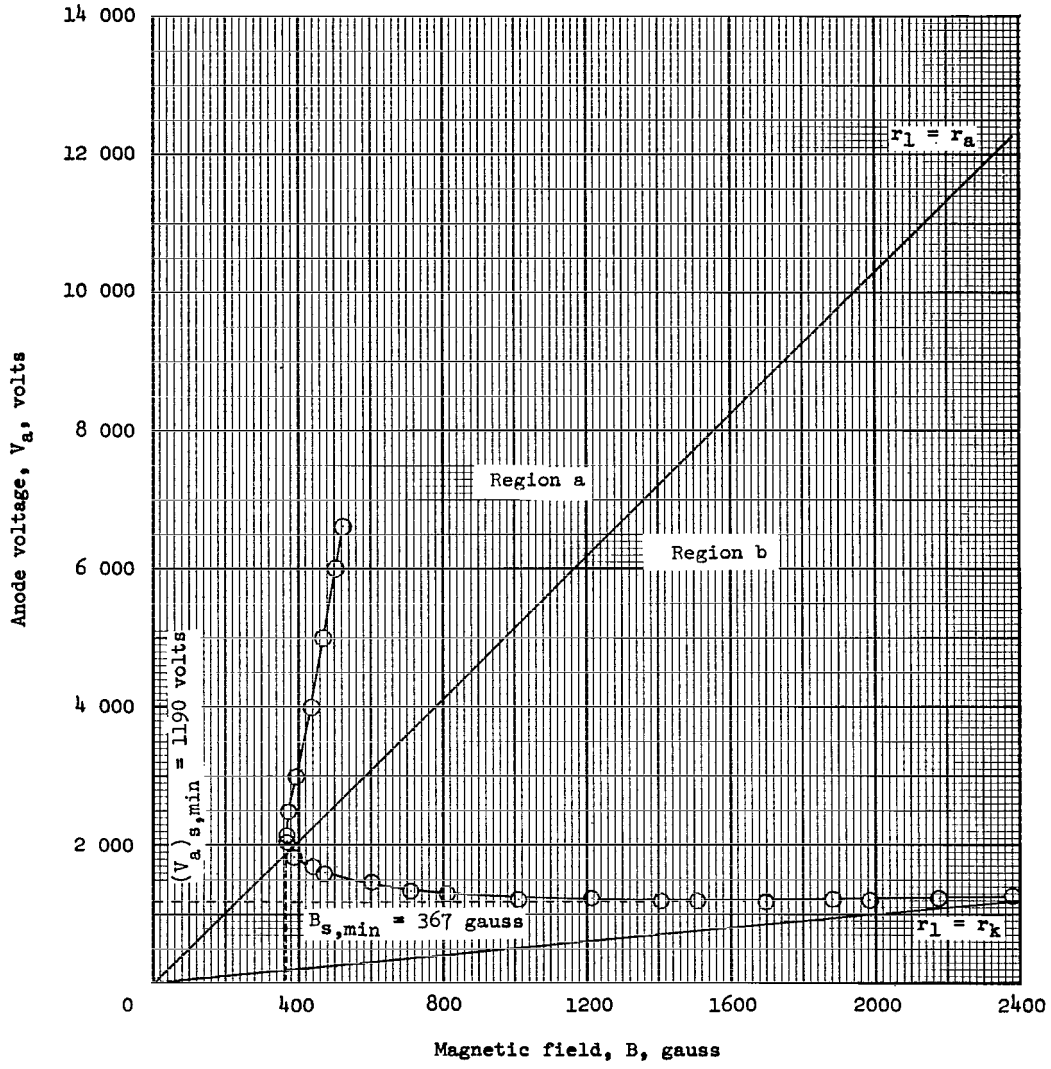

(c) $p = 1.2 \times 10^{-8}$ torr.

Figure 7.- Continued.

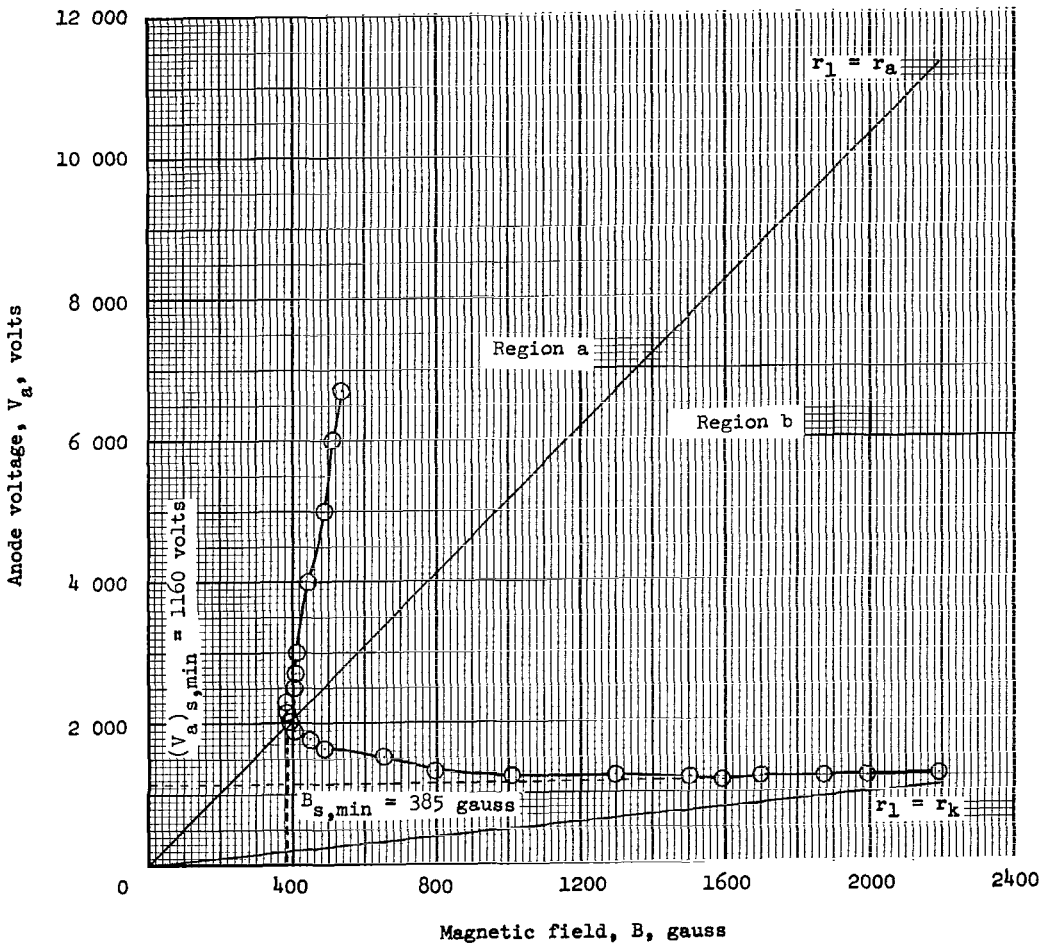

(d) $p = 5.2 \times 10^{-9}$ torr.

Figure 7.- Continued.

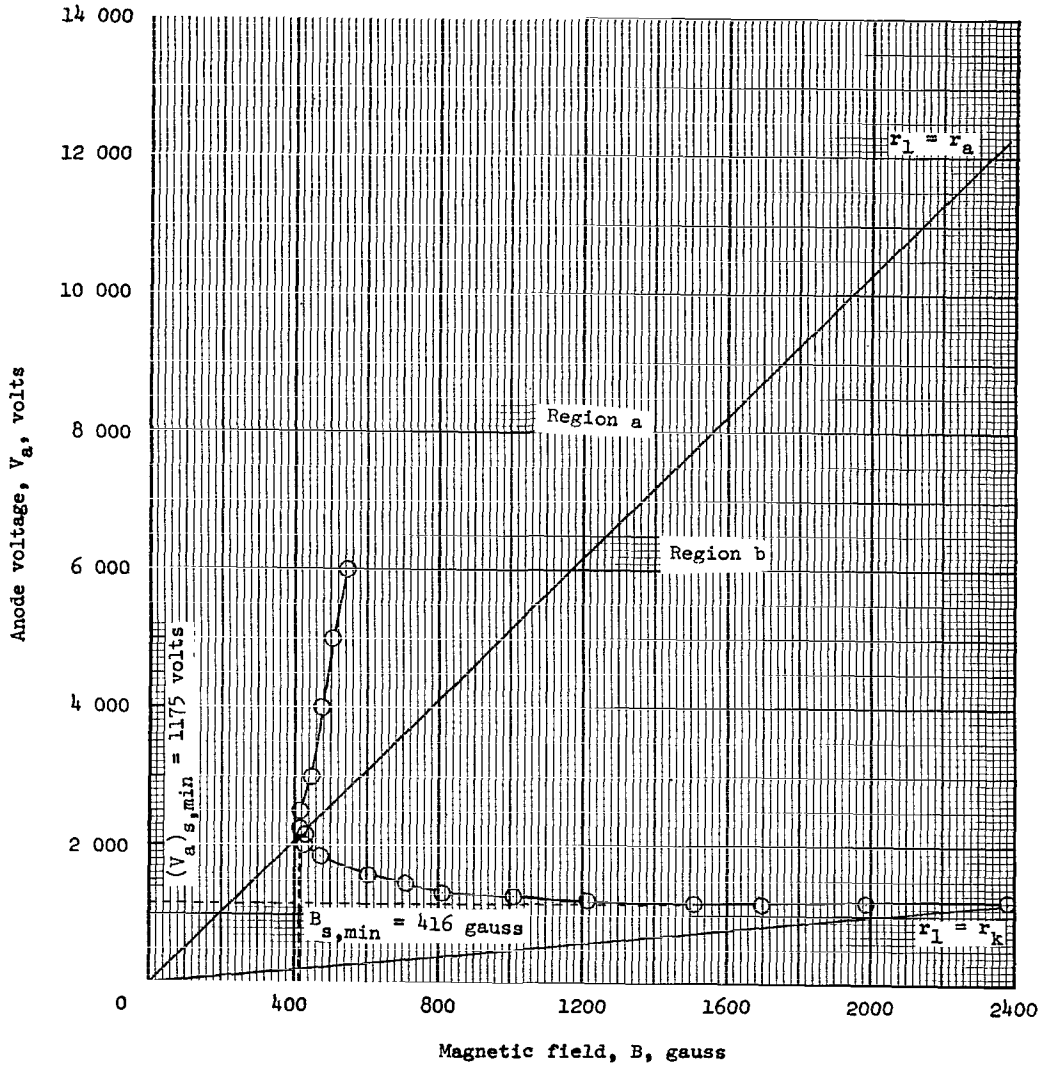

(e) $p = 1.5 \times 10^{-9}$ torr.

Figure 7.- Continued.

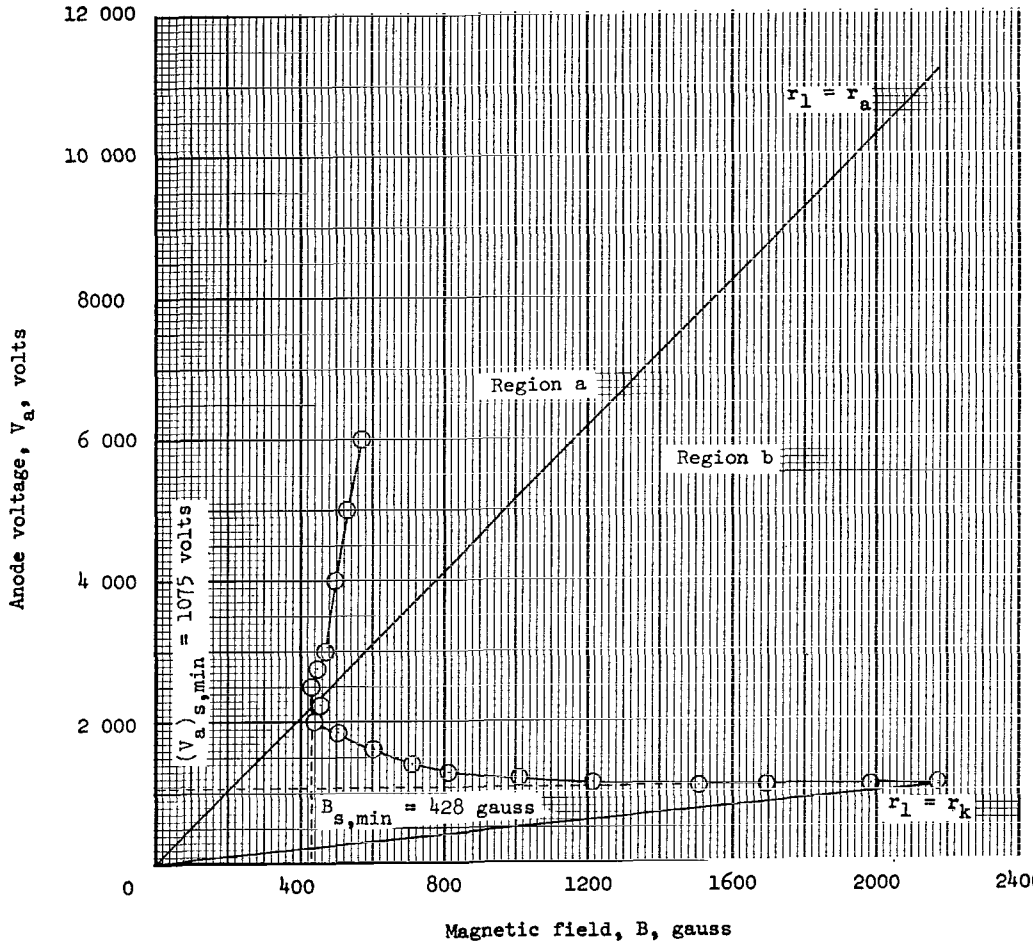

(f) $p = 7.0 \times 10^{-10}$ torr.

Figure 7.- Continued.

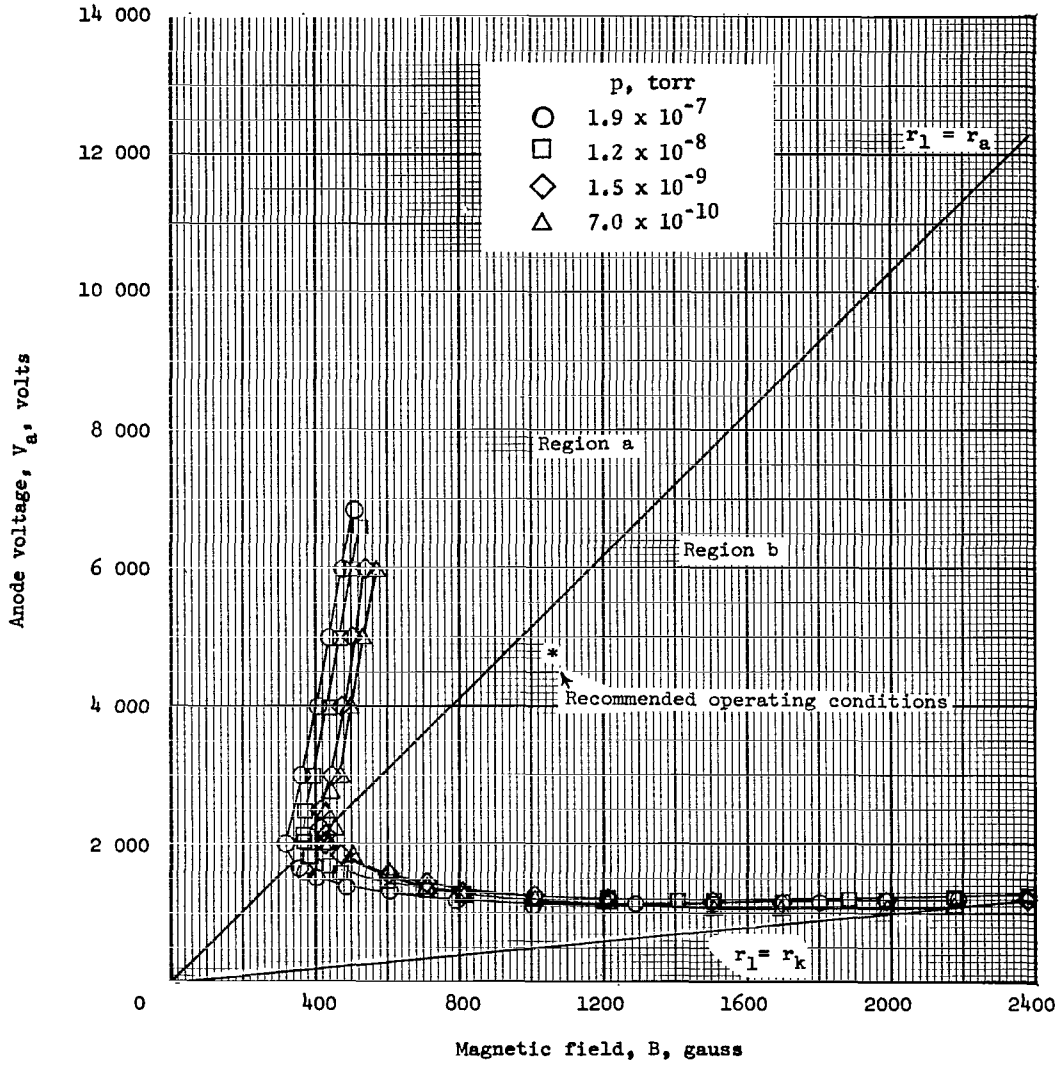

(g) Four representative test pressures.

Figure 7.- Concluded.

Region a

At a given pressure in region a the measured values of the striking characteristics indicate that the striking voltage as a function of magnetic field is not exactly in agreement with the parabolic dependence as predicted by the theory of equation (6), that is, the ratio $(V_a)_s/B_s^2$ is not constant as $(V_a)_s$ increases. Calculated values of the ratio $(V_a)_s/B_s^2$ for various values of $(V_a)_s$ at four representative test pressures are presented in table II. It is obvious that $(V_a)_s/B_s^2$ slightly increases as $(V_a)_s$ increases from 2 to 6 kilovolts. This slight increase in $(V_a)_s/B_s^2$ is believed to be due to an increase in the secondary electron emission coefficient of the cylindrical portion of the cathode γ_k with ion energy. (See appendix A.) As the anode voltage is increased, the ions formed in the interelectrode spacing are accelerated to the cathode with greater energies; thus, greater electron emission per ion impacting the cathode results.

TABLE II.- VARIATION OF $(V_a)_s/B_s^2$ WITH $(V_a)_s$

$(V_a)_s$, volts	$(V_a)_s/B_s^2$, volts/gauss^2
$p = 1.9 \times 10^{-7}$ torr	
3000	0.0225
4000	.0239
5000	.0256
6000	.0260
$p = 1.9 \times 10^{-8}$ torr	
3000	0.0191
4000	.0208
5000	.0228
6000	.0235
$p = 1.5 \times 10^{-9}$ torr	
3000	0.0148
4000	.0177
5000	.0198
6000	.0204
$p = 7.0 \times 10^{-10}$ torr	
3000	0.0137
4000	.0162
5000	.0179
6000	.0183

It is obvious in figure 7(g) that in region a, at a given anode voltage, the striking magnetic field increases as pressure is decreased. This type of behavior has been observed at pressures greater than 1.9×10^{-7} torr. (See ref. 1.) The values of the minimum striking magnetic field in region a were plotted against pressure on a semilog plot as shown in figure 8. The line drawn through the data points is the result of a least squares analysis of the data and shows that the data agree with the theoretical prediction (see eq. 12) which predicts a linear dependence on a semilog plot. It is interesting to note that the data express that, per decade pressure drop, the minimum striking magnetic field increases by a constant amount.

The data shown in figure 8 were used in equation (12) to calculate the effective second Townsend coefficient Γ_k at the points where the minimum striking magnetic fields

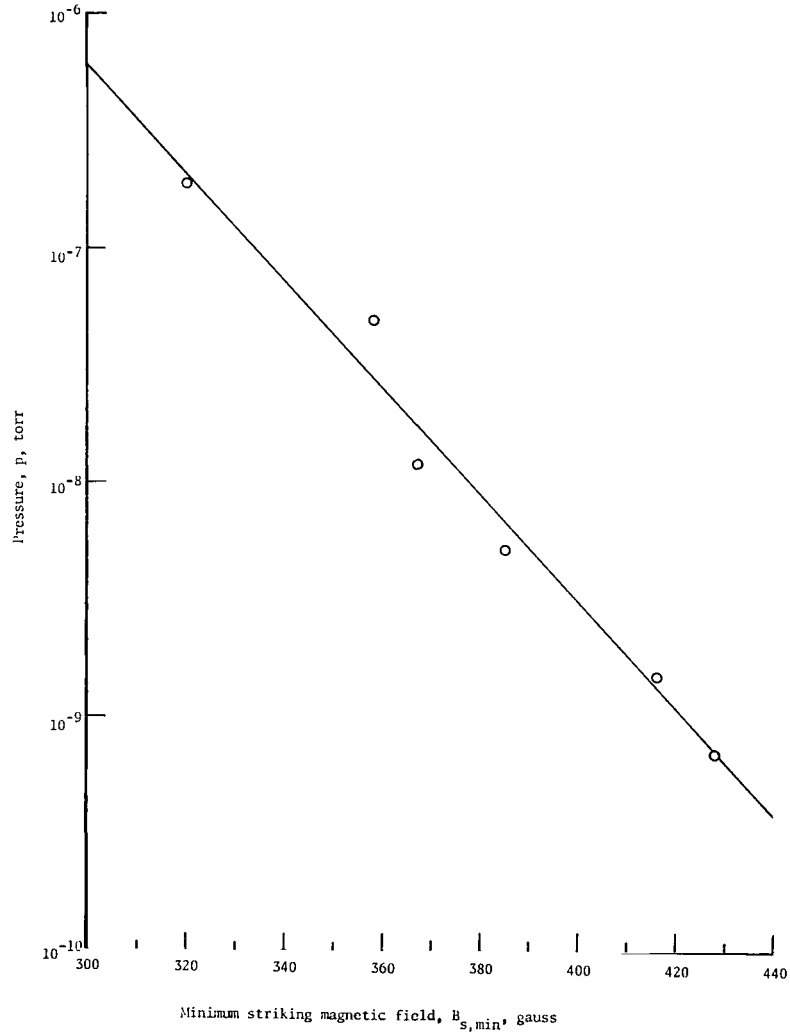

Figure 8.- Variation of minimum striking magnetic field with pressure.

occurred for the various test pressures. Once the Γ_k is known, the intrinsic secondary electron emission coefficient γ_k (see appendix A) can be calculated. Values of γ_k calculated at the points of minimum striking magnetic field for the various test pressures are shown in table III.

TABLE III.- SECONDARY ELECTRON EMISSION COEFFICIENTS AT POINTS OF MINIMUM STRIKING MAGNETIC FIELD

p, torr	γ_k, electrons/ion
1.9×10^{-7}	0.017
5.0×10^{-8}	.020
1.2×10^{-8}	.022
5.2×10^{-9}	.024
1.5×10^{-9}	.024
7.0×10^{-10}	.029

Numerical values of the ratio D_k/r_a were calculated by the constant field theory at the points where the minimum striking magnetic field in region a occurred. The values of this ratio decreased from $D_k/r_a = 0.44$ at $p = 1.9 \times 10^{-7}$ torr (N_2) to $D_k/r_a = 0.26$ at $p = 7 \times 10^{-10}$ torr (N_2).

Since the electric field varies inversely as r, the calculated values of D_k appear to be very large for the assumption of a constant electric field over each cycloid to be a good approximation. Since figure 8 shows that the data agree with the straight-line prediction of equation (12), the assumption of a constant electric field over each cycloid does not introduce disagreement between equation (12) and the experimental data over a pressure range of 1.9×10^{-7} torr (N_2) to 7×10^{-10} torr (N_2).

Region b

In region b at a given pressure, the measurements of the striking characteristics indicate that the striking voltage decreases to a minimum as the magnetic field is increased and then the striking voltage is approximately constant. (See figs. 7(a) to 7(f).) A numerical analysis of the theoretical equation (eq. (15)), a constant effective second Townsend coefficient of the cathode end plates Γ_e being assumed, shows that the striking voltage increases with an increase in magnetic field, after the minimum voltage has occurred. (See fig. 2.) Equation (15) predicts that Γ_e must increase in order for

$(V_a)_s$ to remain approximately constant. Thus, the data indicate that an increase in Γ_e occurs in region b as the striking magnetic field increases. Data at higher pressures (ref. 1) indicate a similar increase in Γ_e with striking magnetic field beyond the minimum striking voltage.

Calculations of the ratio D_k/r_k in region b reveal that at striking magnetic fields greater than 600 gauss, D_k is less than 10 percent of the anode radius and decreases rapidly as the striking magnetic field increases. Thus, the constant electric field assumption over each cycloid should not introduce significant errors in the theoretical prediction of the striking characteristics in region b.

As previously mentioned, at a given pressure, the striking voltage decreases to a minimum as the striking magnetic field increases. This minimum striking voltage for each test pressure (taken from figs. 7(a) to 7(f)) is plotted as a function of pressure as shown in figure 9. The plot shows that the minimum striking voltage as a function of pressure deviates considerably from the theoretical curve of equation (17), which predicts a straight line on a semilog plot. It is not known exactly what causes this large deviation. A change in the dependence of Γ_e on pressure occurs as the ultrahigh vacuum region is approached; this change indicates that some secondary electron-producing mechanism other than that from the cathode end plates may be controlling the discharge.

Striking-Time Lags

At pressures below 5×10^{-8} torr (N_2), striking-time lags occurred. The time-lag data which are presented are those which occurred with the mercury lamp focused on the test gage. The time-lag behavior in region a was similar to the behavior in region b, except that the lags in region b were greater by about a factor of 2. Only time-lag data for region b are presented. Figure 10 shows a plot of the measured time lag t_m against anode voltage for three magnetic field settings in region b at a pressure of 1.5×10^{-9} torr (N_2). The lags at higher and lower pressures are lesser and greater, respectively, and are not shown since the curves of the variation of time lag with anode voltage are similar to those shown in figure 10.

Figure 10 indicates that the time lag increases rapidly as the anode voltage is decreased, and approaches the true striking voltage.

Figure 11 is a plot of the variation of the reciprocal of the measured time lag $(t_m)^{-1}$ with the anode voltage on a linear scale. As $(t_m)^{-1}$ becomes small, the curves appear to become linear with a large slope. Schade (ref. 8) and Loeb (ref. 9) have shown that the time lag for the initiation of a Townsend discharge such as that in the magnetron gage is finite when the true striking voltage is applied. Thus, the true striking voltages

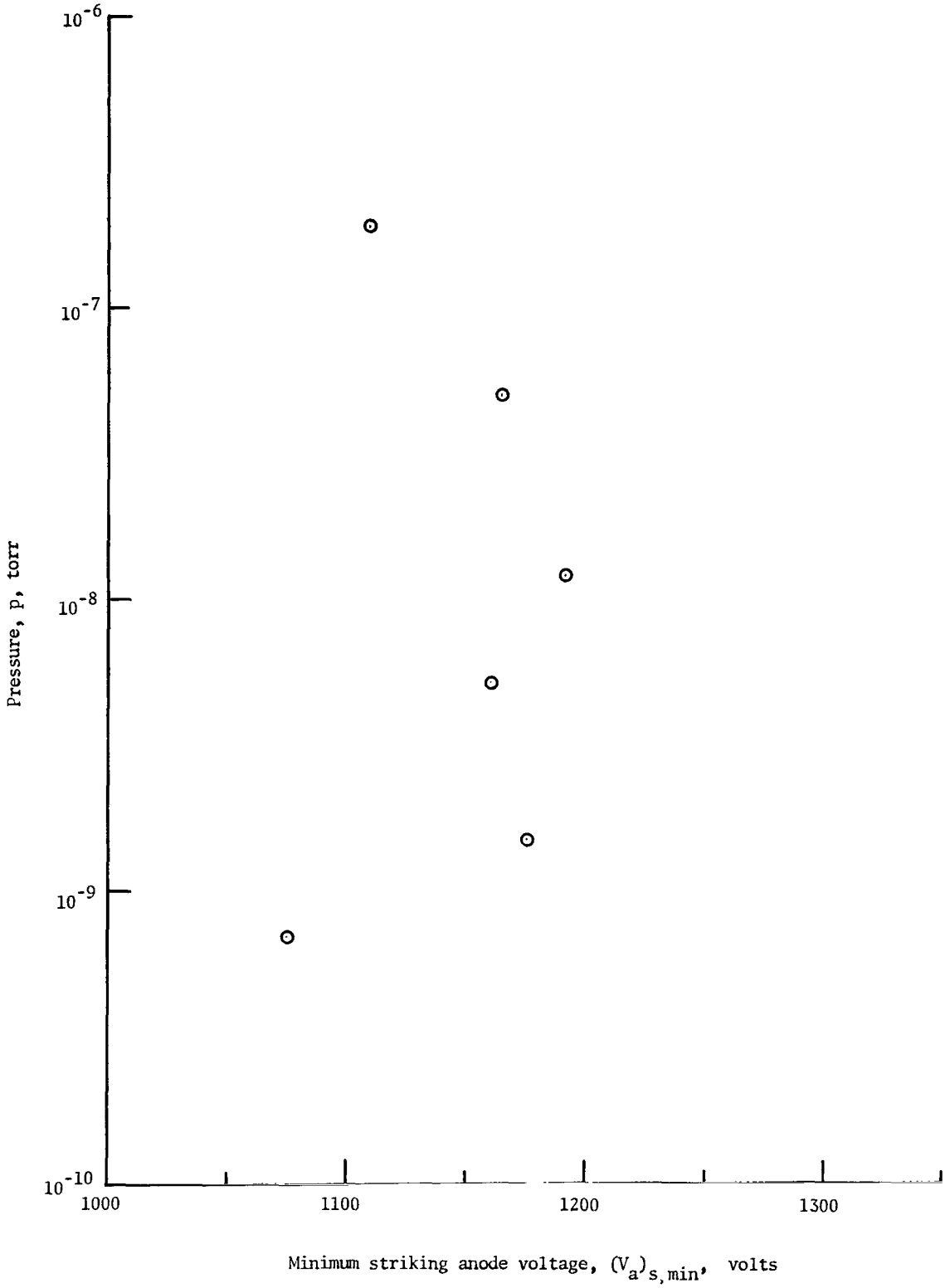

Figure 9.- Variation of minimum striking anode voltage with pressure.

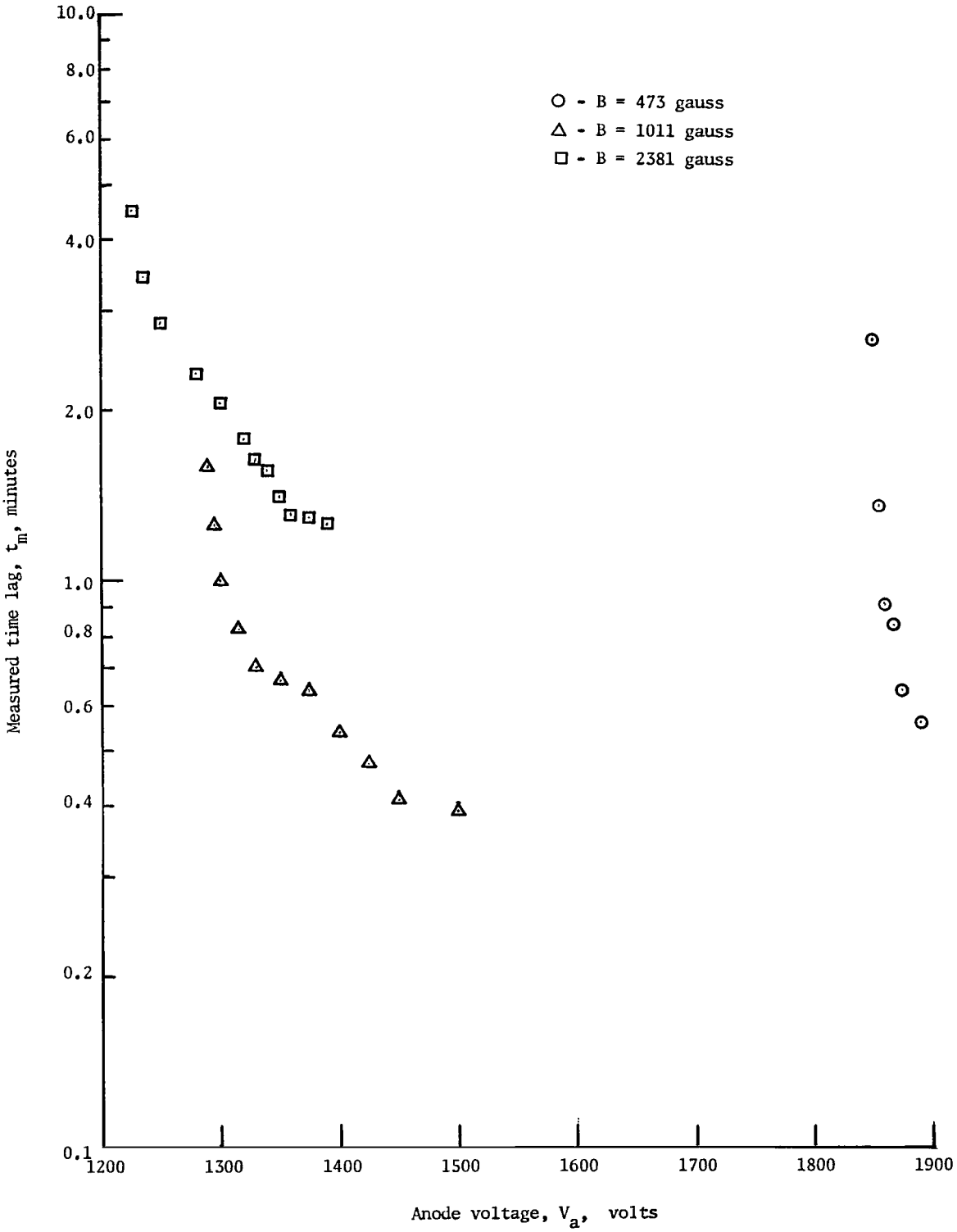

Figure 10.- Variation of measured time lag with anode voltage at $p = 1.5 \times 10^{-9}$ torr for various magnetic fields.

at given pressures and magnetic fields should occur at some value of $(t_m)^{-1} > 0$. The striking voltages measured in this experiment (that is, the striking voltages at which the time lag was greatest) were in all cases within 3 percent of the striking voltages obtained by extrapolation to $(t_m)^{-1} = 0$ of the curves in figure 11 and of the curves typical of figure 11 but not shown.

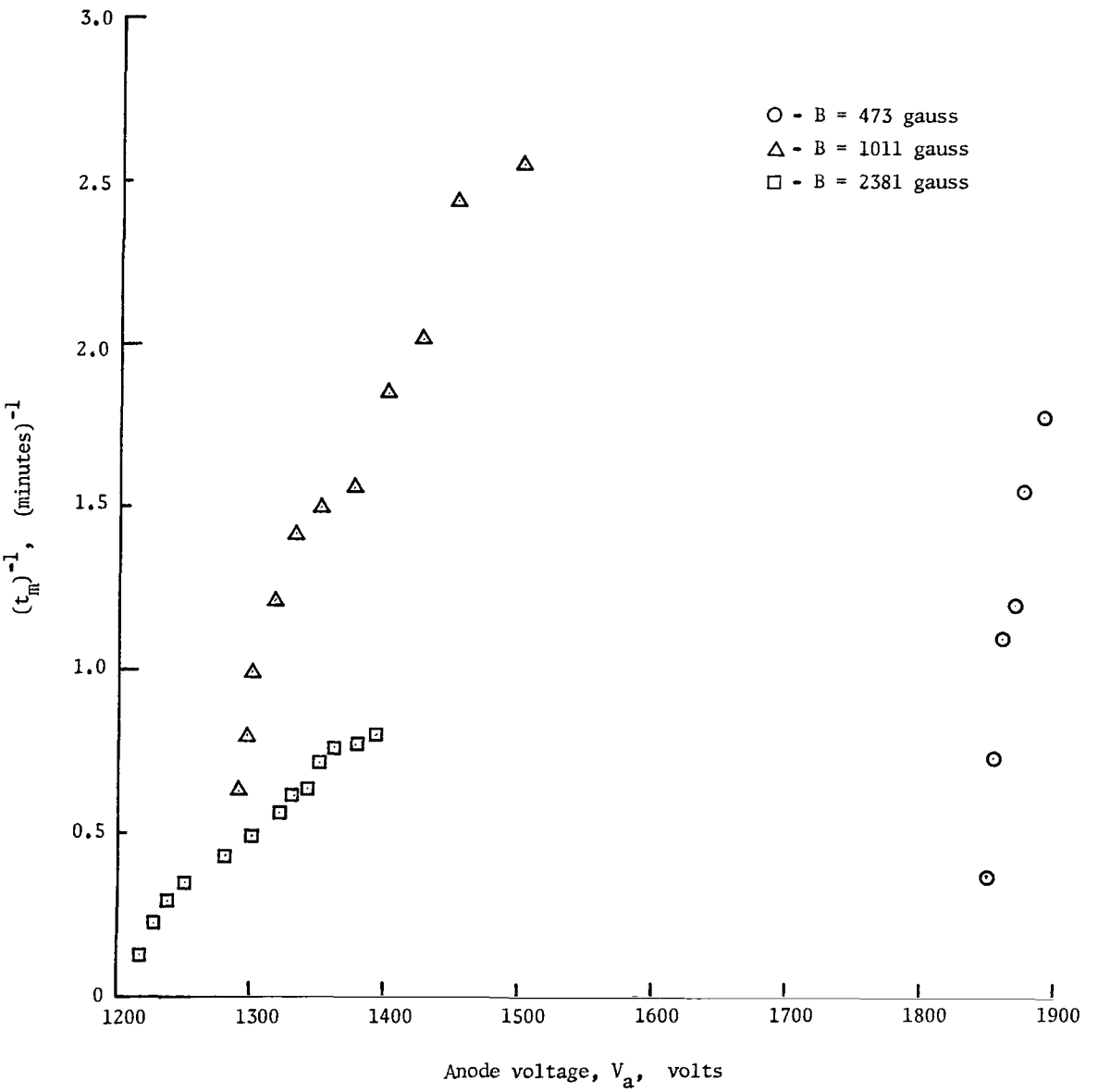

Figure 11.- Variation of $(t_m)^{-1}$ with anode voltage at $p = 1.5 \times 10^{-9}$ torr for various magnetic fields.

In region a, the time lags and $(t_m)^{-1}$ were plotted against the striking magnetic field and the curves were very similar to the curves plotted for region b. The measured striking magnetic fields (striking magnetic field at which the time lags were greatest) were all within 3 percent of the values obtained by extrapolation of the curves of $(t_m)^{-1}$ plotted against B_s to $(t_m)^{-1} = 0$. Thus, the occurrence of time lags did not contribute significant errors in the measurements of the striking characteristics in regions a and b.

CONCLUSIONS

An investigation of the striking characteristics of the magnetron ionization gage in helium over the pressure range of 1.9×10^{-7} torr (N_2) to 7×10^{-10} torr (N_2) has been conducted. The following conclusions were reached:

1. The manufacturer's recommended operating conditions of the magnetron gage (Anode voltage $\approx$ 4800 volts, Magnetic field strength $\approx$ 1050 gauss) are well within the boundaries or lower limits of operation over the pressure range of the investigation.

2. The measured striking characteristics in the upper branch of the striking characteristics diagram deviate slightly from the theoretical parabolic prediction in that the ratio of the striking anode voltage and the square of striking magnetic field $(V_a)_s/B_s^2$ increases as $(V_a)_s$ increases. This deviation from theory is possibly due to an increase in the secondary-electron-emission coefficient of the cylindrical portion of the cathode γ_k with ion energy.

3. A constant increase in the minimum striking magnetic field in the upper branch of the striking characteristics diagram occurs per decade pressure drop over the pressure range of the investigation. This observed movement of the minimum striking magnetic field is in agreement with the Townsend breakdown theory which assumes a constant electric field over each cycloid.

4. On the lower branches of the striking characteristics diagram, the striking voltage decreases to a minimum as the striking magnetic field increases, and then remains approximately constant as the striking magnetic field increases further.

5. The dependence of the minimum striking voltage on pressure for the lower branches of the striking characteristics diagram deviates considerably from the theoretical prediction. This deviation is probably due to the significant contribution of some mechanism controlling the discharge other than secondary electron emission from the cathode end plates. Otherwise, in the lower branch, the data substantiate the proposed theory for the breakdown of the gage and show that the behavior of the striking characteristics at pressures in the region investigated conforms with the behavior at higher pressures.

6. Striking time lags of the magnetron gage become larger as the pressure is decreased into the ultrahigh vacuum region, but do not contribute significant errors in the measurements of the striking characteristics.

Langley Research Center,
National Aeronautics and Space Administration,
Langley Station, Hampton, Va., March 14, 1968,
124-09-19-01-23.

APPENDIX A

ELECTRON MOTION AND TOWNSEND COEFFICIENTS

The theory section of this paper does not describe in detail either the electron motion leading to breakdown in the gage or the major ionization processes occurring in the gage. To aid the reader in more fully understanding the theory, this appendix contains discussion of the following topics: (1) Electron motion leading to the establishment of the breakdown condition (eq. (3)) within the gage, (2) explanation of the first Townsend coefficient, α, and (3) derivation of the second Townsend coefficients, Γ_k and Γ_e.

Electron Motion

Electrons can be emitted from the cathode of the magnetron gage by photoelectric and/or field emission. The field emission results from the voltage being placed on the anode. Once emitted, an electron is subjected to the electrostatic and Lorentz forces. The equation of motion of the electron in the presence of the radial electric field and uniform magnetic field is

$$m\frac{d\vec{v}}{dt} = -e\left(\vec{E} + \vec{v} \times \vec{B}\right) \tag{18}$$

The solution to equation (18) shows that the trajectories of the emitted electrons are cycloidal if no collisions take place. (See fig. 1 and ref. 10.) The velocity $\vec{v}$ can be decomposed into two velocities

$$\vec{v} = \vec{v}_r + \vec{v}_\theta \tag{19}$$

where v_r is a rotating velocity and represents a circular motion about a magnetic line of force (cyclotron motion), and

$$\left|\vec{v}_\theta\right| = \frac{E}{B} \tag{20}$$

is the constant drift velocity.

Several assumptions other than the three mentioned in the theory section are made in developing the theory of electron motion in the magnetron gage when collisions with gas molecules occur. These assumptions are made in order to simplify the analysis. The assumptions are: (1) the thermal velocity of neutrals is much smaller than the average electron velocity; (2) an electron is at rest after an ionizing collision with a gas molecule; (3) the mean free path of an electron is independent of velocity; and

(4) electrons can be elastically scattered. After being elastically scattered, the electrons are at rest; all elastically scattered electrons are capable of ionization.

The electrons emitted from the cathode have no systematic motion parallel to the electric field. For the occurrence of such motion the electrons must perform collisions with the gas molecules. In this way the electrons can jump in radial directions from one magnetic field line to another, and thus approach the anode.

The condition for ionization is given by equation (7). Ionization by an electron colliding with a gas molecule produces an ion and an additional electron (ion pair). The electrons emitted from the cathode travel over half of a cycloid and fall back to the cathode unless they collide with and ionize a gas molecule. The electrons experiencing these ionizing collisions are assumed to return to zero velocity and to start their cycloidal motion again from the point of collision. These electrons and others formed in the interelectrode spacing are trapped indefinitely in hypocycloidal orbits until they experience further collisions with gas molecules. At each additional ionizing collision, the electron returns to zero energy and restarts its cycloidal motion from a point closer to the anode. Thus, electrons can only progress toward the anode by successive collisions with gas molecules. The growth of the ionization process in the interelectrode spacing is exponential in the r-direction. The total number of ion pairs formed by one electron traveling in the direction of the electric field is

$$n = \exp \int_{r_k}^{r_1} \alpha \, dr \tag{21}$$

The $\exp \int_{r_k}^{r_1} \alpha \, dr$ positive ions formed drift to the cathode. Upon impacing the cathode, these ions cause secondary electron emission from the cathode. The total number of secondary electrons emitted from the cathode capable of ionizing gas molecules is

$$n = \Gamma \exp \int_{r_k}^{r_1} \alpha \, dr \tag{22}$$

It can be shown (ref. 9) by using equations (21) and (22) that the current flowing in a nonuniform electric field is

$$i = i_o \frac{\exp \int_{r_k}^{r_1} \alpha \, dr}{1 - \Gamma\left(\exp \int_{r_k}^{r_1} \alpha \, dr - 1\right)} \tag{23}$$

APPENDIX A

When the condition

$$\Gamma\left(\exp \int_{r_k}^{r_1} \alpha \, dr - 1\right) = 1 \tag{24}$$

prevails, equation (23) is indeterminate. Equation (3) in the theory is determined by taking the logarithm of both sides of equation (24). According to the theory originally suggested by Townsend, this condition defines the onset of breakdown. In general, at the value of α corresponding to breakdown, $e \int_{r_k}^{r_1} \alpha \, dr >> 1$, so that equation (24) becomes

$$\Gamma \exp \int_{r_k}^{r_1} \alpha \, dr = 1 \tag{25}$$

The significance of the breakdown condition (ref. 9) is that when the number $\exp \int_{r_k}^{r_1} \alpha \, dr$ of ion pairs produced in the interelectrode spacing is sufficiently large to permit the positive ions, on bombarding the cathode, to release one secondary electron and cause a repetition of the process, the discharge is self-sustaining and can continue in the absence of i_o.

First Townsend Coefficient, α

The first Townsend coefficient α is the number of ion pairs formed per electron per centimeter travel of an electron in the direction of the electric field. Investigations have been devoted to calculations of α (refs. 5, 11, 12, and 13), but only one of these (ref. 5) considers the contribution to α made by those electrons which have been elastically scattered. Equation (4) is the result of the calculation of reference 5 and is used in this paper in developing the theory. No analysis of the development of α will be given in this paper as it is clearly presented in reference 5.

Second Townsend Coefficient, Γ

The second Townsend coefficient Γ is the number of electrons reentering the discharge per ion leaving the discharge. This coefficient can be expressed as

$$\Gamma = \gamma \psi \tag{26}$$

(from ref. 5) where γ is the total number of secondary electrons emitted per ion impacting the cathode and ψ is the probability that an electron will suffer a collision.

APPENDIX A

The probability that an electron, once emitted from the cathode, will travel over its first cycloid without suffering a collision is (from ref. 5),

$$\psi_k' = \exp\left(\frac{-4D_k}{\lambda}\right) \tag{27}$$

Thus, the probability that an electron will suffer a collision is

$$\psi_k = \left[1 - \exp\left(\frac{-4D_k}{\lambda}\right)\right] \tag{28}$$

Equation (26) becomes

$$\Gamma = \gamma\left[1 - \exp\left(\frac{-4D_k}{\lambda}\right)\right] \tag{29}$$

If $\frac{4D_k}{\lambda} << 1$, equation (29) reduces to

$$\Gamma = \frac{4\lambda D_k}{\lambda} \tag{30}$$

With the use of the expression for D (eq. (10)), Γ can be expressed as

$$\Gamma = \psi_k \gamma = \frac{8\gamma E_k}{\eta \lambda B^2} \tag{31}$$

Equation (30) holds true for the second Townsend coefficient of the cylindrical portion of the cathode Γ_k; thus,

$$\Gamma_k = \frac{4\gamma_k D_k}{\lambda} \tag{32}$$

The expression for Γ_e is similar to equation (30), but differs in that the characteristic path length, equivalent to $4D_k$ in equation (30), is approximately equal to the distance between the cathode end plates l. (See ref. 5.) Thus,

$$\Gamma_e \approx \frac{\gamma_e l}{\lambda} \tag{33}$$

for $\frac{l}{\lambda} << 1$.

REFERENCES

1. Redhead, P. A.: The Magnetron Gauge: A Cold-Cathode Vacuum Gauge, Can. J. Phys., vol. 37, no. 11, Nov. 1959, pp. 1260-1271.

2. Feakes, F.; Torney, F. L., Jr.; and Brock, F. J.: Gauge Calibration Study in Extreme High Vacuum. NASA CR-167, 1965.

3. Kreisman, W. S.; and Herzog, R.: Development of Cold Cathode Ionization Gauges for the Measurement of Low Pressures. GCA Tech. Rep. 61-18-N (Contract No. NAS5-270), Geophys. Corp. Amer., Nov. 1961.

4. Mechtly, E. A.: The International System of Units – Physical Constants and Conversion Factors. NASA SP-7012, 1964.

5. Redhead, P. A.: The Townsend Discharge in a Coaxial Diode With Axial Magnetic Field. Can. J. Phys., vol. 36, no. 3, Mar. 1958, pp. 255-270.

6. Haefer, R.: Über den Mechanismus der Zündung einer Elektrischen Gasentladung unter der Einwirkung eines transversalen Magnetfeldes im Druckbereich 10^{-1} bis 10^{-8} torr. Acta Phys. Austr., Bd. 7, Heft 3, July 1953, pp. 251-277.

7. Outlaw, R. A.; and Bradford, James M., Jr.: A Small Volume, Ultrahigh Vacuum System for Ionization Gage Studies. NASA TN D-4208, 1967.

8. Schade, Rudolf: The Time of Formation of a Glow Discharge. Z. Physik, vol. 104, 1937, pp. 489-510.

9. Loeb, Leonard B.: Statistical Factors in Spark Discharge Mechanisms. Rev. Mod. Phys., vol. 20, no. 1, Jan. 1948, pp. 151-160.

10. Schuurman, W.: Investigation of a Low-Pressure Penning Discharge. Rijnhuizen Rep. No. 66-28, Ass. Euratom-Fom Fom-Inst. Plasma-Fys. (Ned.), Mar. 1966.

11. Meek, J. M.; and Craggs, J. D.: Electrical Breakdown of Gases. The Clarendon Press (Oxford), 1953.

12. Somerville, J. M.: Sparking Potentials in a Transverse Magnetic Field. Proc. Phys. Soc. (London), vol. 65, pt. 8, no. 392B, Aug. 1, 1952, pp. 620-629.

13. Haefer, R.: Die Zündspannung von Gasentladungen unter dem Einfluss eines transversalen Magnetfeldes im Druckbereich von 10 bis 10^{-8} Torr. Acta Phys. Austr., Bd. 7, Heft 1, Apr. 1953, pp. 52-90.

NATIONAL AERONAUTICS AND SPACE ADMINISTRATION
WASHINGTON, D.C. 20546

OFFICIAL BUSINESS

FIRST CLASS MAIL

POSTAGE AND FEES PAID
NATIONAL AERONAUTICS AND
SPACE ADMINISTRATION

POSTMASTER: If Undeliverable (Section 158 Postal Manual) Do Not Return

"The aeronautical and space activities of the United States shall be conducted so as to contribute . . . to the expansion of human knowledge of phenomena in the atmosphere and space. The Administration shall provide for the widest practicable and appropriate dissemination of information concerning its activities and the results thereof."

— NATIONAL AERONAUTICS AND SPACE ACT OF 1958

NASA SCIENTIFIC AND TECHNICAL PUBLICATIONS

TECHNICAL REPORTS: Scientific and technical information considered important, complete, and a lasting contribution to existing knowledge.

TECHNICAL NOTES: Information less broad in scope but nevertheless of importance as a contribution to existing knowledge.

TECHNICAL MEMORANDUMS: Information receiving limited distribution because of preliminary data, security classification, or other reasons.

CONTRACTOR REPORTS: Scientific and technical information generated under a NASA contract or grant and considered an important contribution to existing knowledge.

TECHNICAL TRANSLATIONS: Information published in a foreign language considered to merit NASA distribution in English.

SPECIAL PUBLICATIONS: Information derived from or of value to NASA activities. Publications include conference proceedings, monographs, data compilations, handbooks, sourcebooks, and special bibliographies.

TECHNOLOGY UTILIZATION PUBLICATIONS: Information on technology used by NASA that may be of particular interest in commercial and other non-aerospace applications. Publications include Tech Briefs, Technology Utilization Reports and Notes, and Technology Surveys.

Details on the availability of these publications may be obtained from:

SCIENTIFIC AND TECHNICAL INFORMATION DIVISION

NATIONAL AERONAUTICS AND SPACE ADMINISTRATION

Washington, D.C. 20546